

# Estimating the commercial volume of a *Pinus taeda* L. plantation using active and passive sensors

Carla Talita Pertille<sup>1\*</sup>, Marcos Felipe Nicoletti<sup>2</sup>, Mario Dobner Jr<sup>2</sup>

<sup>1</sup>Federal University of Parana, Brazil  
<sup>2</sup>State University of Santa Catarina, Brazil

SILVICULTURE

## ABSTRACT

**Background:** The objective of this study was to estimate the wood volume of a *Pinus taeda* L. plantation using variables extracted from the Sentinel-1 active sensor and the Sentinel-2 passive sensor. To do so, data from a forest inventory with rectangular plots of 550 m<sup>2</sup> were used to estimate the stand volume. We derived and adapted average vegetation indices per plot from images obtained by Sentinel-1 and Sentinel-2 sensors. The data were then correlated with the volume per plot based on the forest inventory. The Modified Radar Forest Degradation Index (mRDFI) showed the highest correlation for Sentinel-1 data, while the Difference Vegetation-Index (DVI) performed best for Sentinel-2.

**Results:** The regression models were built using Stepwise modeling, demonstrating that the models fit with only the Sentinel-2 indices performed better than the others (indices adapted for Sentinel-1 and a combination of Sentinel-1 and Sentinel-2 data), with an R<sup>2</sup> adjusted between 0.51 to 0.40 and a standard error (Syx%) of 3.66 to 8.97. According to the statistical analyses, we found no significant differences between the volume estimated by the forest inventory (12.56±1.17) and the remote sensing techniques used (Sentinel-2 with 12.56±1.03 and Sentinel-1 with 12.56±0.94). However, further tests should be conducted with other active sensors operating in different spectral bands and polarization modes for other forest species.

**Conclusion:** We found no significant differences between the volumetric estimates derived from remote sensing data and forest inventory techniques.

**Keywords:** modeling, Sentinel-1, Sentinel-2, wood stock.

## HIGHLIGHTS

There was no significant difference between the volumetric estimates derived from remote sensing data and forest inventory techniques, but the regression model built with Sentinel-2 was the most suitable for estimating the volume of *Pinus taeda* L.

PERTILLE, C.T.; NICOLETTI, M.F.; DOBNER JR, M. Estimating the commercial volume of a *Pinus taeda* L. plantation using active and passive sensors. CERNE, v.29, e-103108, doi: 10.1590/01047760202329013108.

\*Corresponding author: carla.pertille@ufpr.br

Received: May, 24 2022

Accepted: December, 2 2022



## INTRODUCTION

According to data from the Brazilian Tree Industry (Ibá, 2021), there are 1.7 million hectares of *Pinus* spp. plantations across the country. The majority of these are concentrated in the South, making up 67% of all planted pine forests (43% in Paraná and 24% in Santa Catarina State). This fact highlights the significant adaptability of the genus, especially in the southern region of Brazil, with similar edaphoclimatic characteristics to the origins of several pine species (Ferro et al., 2018). Given the importance of commercial forest plantations, particularly those of the *Pinus* genus, it is essential to use accurate forest inventory methodologies to obtain and evaluate forest attributes, such as volume and biomass, to support forest management strategies and to implement climate change mitigation policies (Mauya et al., 2015). The accuracy of wood volume estimates in forest surveys is related to the sampling technique, as well as the choice of the method used, which can be direct (cubic scaling or weighing of the tree) or indirect (volumetric equations, form factor applications, and tapering equations) (Leal et al., 2013).

Forest inventory methods to quantify the volume of forest plantations are widely used and highly effective; however, some factors make difficult their implementation, such as the labor cost, the time required, the availability of adequate equipment, and difficulties operating in dense forests and those which are difficult to access (Berra et al., 2012). Thus, combining such procedures with other techniques and data sources, such as remote sensing, are necessary. Macedo et al. (2017) note that image-derived reflectance information through remote sensing is combined with stand data obtained in the field to estimate the commercial volume of a forest stand. The authors also suggest the use of vegetation indices for such correlations by evaluating and analyzing the spectral properties of vegetation related to vegetation cover, biomass, and leaf area index, particularly in the visible and infrared ranges (Ponzoni et al., 2012).

The evolution of remote sensing technologies has led to the emergence of techniques, sensors, and data acquisition platforms, that enable the integration of different data sources, such as the combined use of optical sensor images and active Radio Detection and Ranging (Radar) sensors, to maximize the potential and complement the limitations of different sensors as compared to other methods (Shao and Zang, 2016). Such combinations favor applying different types of analyses, as Synthetic Aperture Radar (SAR) sensors can produce images independent of daylight or atmospheric conditions, unlike optical sensors which are influenced by atmospheric conditions and cloud coverage (Mauya et al., 2019). In this context, the Sentinel mission deployed by the European Space Agency (ESA) stands out as it provides optical images from the Sentinel-2 satellite, as well as Radar images from the Sentinel-1 satellite. Both satellites have a catalogue of openly available images from around the globe. The sensors of Sentinel-1 operate in the C-band with dual polarization, providing images with 12-day temporal resolution (Torres

et al., 2012). On the other hand, Sentinel-2 offers images with 13 spectral bands at 10 meters (m), 20 m, and 60 m of spatial resolution, and a temporal resolution of five to 10 days (ESA, 2022a). In this scenario, the objective of this study was to compare the commercial volume estimates of a *Pinus taeda* L. plantation using Radar images (Sentinel-1) and optical images (Sentinel-2) with traditional forest inventory methodologies.

## MATERIAL AND METHODS

### Description of the study area

The study was conducted in a rural property located in the municipality of Rio Negro, Paraná, Brazil (geographical coordinates: 26°11'06" South and 49°33'11" West) (Figure 1). The study area is located in the Segundo Planalto Paranaense, predominantly formed by sedimentary units of the Paraná Basin, with Tb allic cambisol and allic litholic soils. The area's climate is Cfa with a dry and temperate climate according to the Koppen classification. Temperatures range between 9°C and 28°C, and the average annual rainfall is 1200 mm (Alvares et al., 2013). The evaluated stand has an effective planting area of 27.5 ha, with *Pinus taeda* L. individuals of 11 and 12 years of age, a spacing of 3 x 2.5 m, and 1,333 trees per hectare.

### Data collection

Forest inventory information was used to guide data collection from rectangular plots of 550 m<sup>2</sup> in April 2021, and measured the following dendrometric variables: diameter at breast height (DBH; cm) using a dendrometric tape measure; and height (m) of 20% of all trees in the plot using a Vertex hypsometer. The Curtis hypsometric equation was later used to obtain the height of all trees in the 48 plots. We used the 5-degree tapering function (Schöpfer model) and cubic data of 72 trees from different diametric classes to determine volume, measuring 0.1 m, 0.5 m, 1.0 m, 1.3 m, 1.5 m, 2.0 m, and subsequent height intervals of 2.0 m until the top of the tree. Table 1 contains the main dendrometric characteristics of the evaluated stand.

### The sentinel mission

Images from the Sentinel-1 active sensor and Sentinel-2 passive sensor were used for remote sensing data. The Sentinel-1 image was acquired free of charge from the Alaska Satellite Facility (ASF, 2022), dated 10/04/2021, with a 12-day temporal resolution, in C-band, Interferometric Wide Swath Mode (IW), level 1C, Single Look Complex (SLC) product, dual polarization VH (vertical transmission and horizontal reception) and VV (horizontal transmission and reception), and a spatial resolution of 5 to 20 m (ESA, 2022b). It acquires data with a 250 km swath at 5 m by 20 m spatial resolution (single look) (ESA, 2022b).

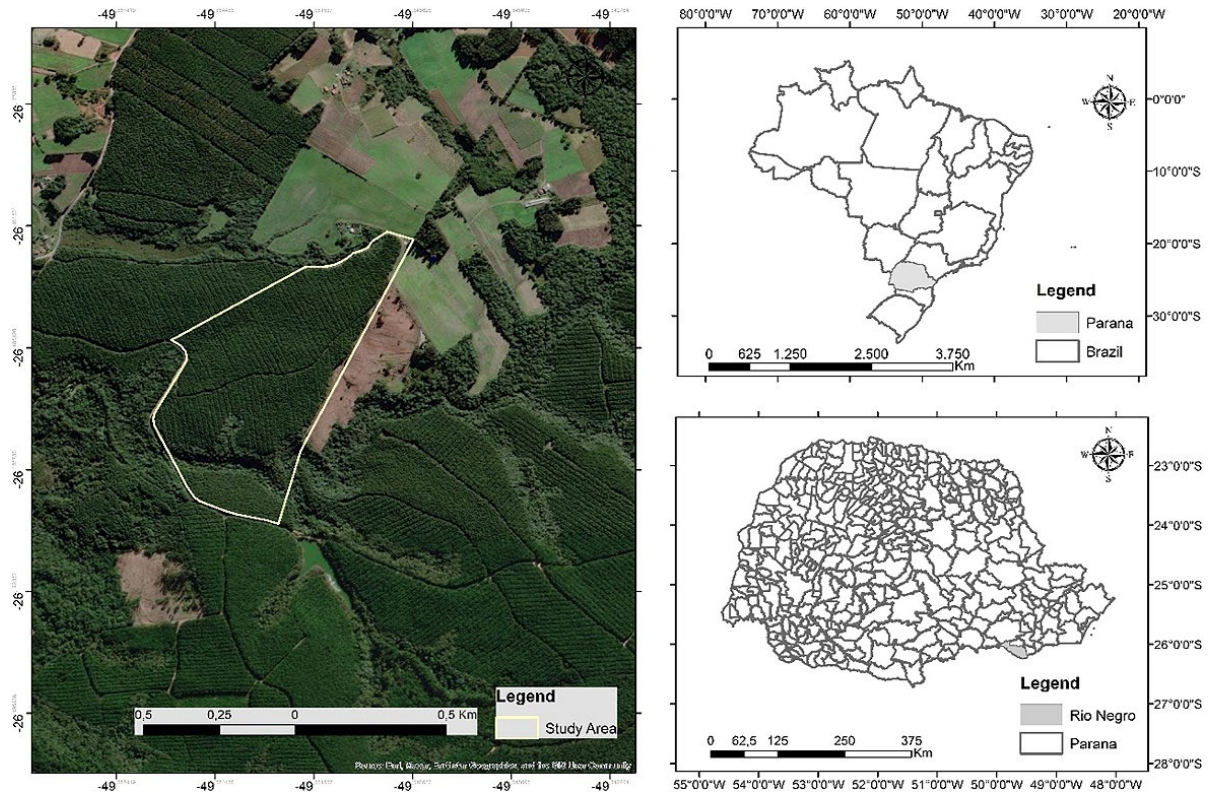


**Figure 1.** Location of a *Pinus taeda* L. stand located in Rio Negro, Paraná, Brazil.

**Table 1.** Descriptive statistics of the dendrometric variables of a *Pinus taeda* L. plantation located in Rio Negro, Paraná, Brazil.

Statistic	DBH	H	G	V
Minimum	24.3	15.8	32.0	172.8
Mean	26.3	17.4	39.8	228.5
Maximum	28.6	18.5	45.5	273.3
Range	4.4	2.7	13.5	100.5
Standard deviation	1.1	0.6	2.8	21.5
Coefficient of variation (%)	4	4	7	9

DBH: diameter at breast height (cm); H: height (m); G: basal area per hectare (m<sup>2</sup>.ha<sup>-1</sup>); V: volume per hectare (m<sup>3</sup>.ha<sup>-1</sup>).

The digital processing of the Sentinel-1 image was performed in the Sentinel Application Platform (SNAP) computer application (ESA, 2022c). The first processing step was to extract the area of interest contained in the IW strips. Then, the orbit correction was performed from the metadata of the image such as the satellite precision and speed. After that, the existing thermal noise was removed and the images were calibrated with the sigma band. Later, the bursts were unified using the Deburst option. The Lee filter was used to reduce the Speckle effect, the dimensions of the regular pixels were applied, and the GR Square Pixel method was used to reduce the size of the pixels. Finally, the terrain distortions were adjusted by the Range Doppler Terrain Correction function using the Bilinear function for the interpolation to obtain the backscatter

coefficients (VH and VV). These data were then exported to a GIS environment (ESRI, 2022), in which vegetation indices adapted for Sentinel-1 images were derived (Table 2).

**Table 2.** Extracted variables from the Sentinel-1 image for a *Pinus taeda* L. stand.

Adapted index	Formula	Reference
mRFDI	$\frac{VV - VH}{VV + VH}$	Nicholas et al. (2021)
RVI	$\frac{8 * VH}{VV + VV + 2 * VH}$	Flores-Andersen et al. (2019)
RVIad	$\frac{4 * VH}{VV + VH}$	This study
Ad_1	$\frac{VV}{VH}$	This study
Ad_2	$\frac{VH}{VV}$	This study
Ad_3	$\frac{1}{VH} + \frac{1}{VV}$	This study
Ad_4	$\frac{1}{VH} / \frac{1}{VV}$	This study
Ad_5	$VH - VV$	This study

VV and VH: backscatter coefficients; mRFDI: Modified Radar Forest Degradation Index; RVI: Radar Vegetation Index; RVIad: Radar Vegetation Index Adapted; Ad\_1, Ad\_2, Ad\_3, Ad\_4, and Ad\_5: adaptations developed in this study.

It is important to highlight that the RVIad index was derived from the RVI index constructed by Çolak, Chandra and Sunar (2021) with the aim of monitoring aboveground biomass. The image derived from the Sentinel-2 satellite to use remote sensing data was obtained from the USGS portal (2022), dated 04/25/2021, in 1C mode, meaning it only had radiometric calibrations. As a result, the atmospheric correction was performed using the Sen2Cor algorithm in SNAP and the image was later submitted to the resampling step of the bands to 10 m. Once the image was properly processed, 14 vegetation indices (Table 3) and three biophysical vegetation parameters were calculated (Leaf Area Index – LAI; Fraction of Absorbed Photosynthetically Active Radiation – Fapar; and Fraction of Vegetation Cover – FVC) with the aid of the PROSAIL model in SNAP (Esa, 2022c).

After obtaining the variables derived from the Sentinel-1 and Sentinel-2 images, the next step was to delimit the forest inventory plots in the images. To do so, we created

areas of influence based on the central coordinates (obtained with the help of Tablet devices with Forest Mobile software) of the plots with a radius of 13.25 meters, for a total of approximately 550 m<sup>2</sup>. Then, the mean values of the variables (Sentinel-1 and Sentinel-2) were extracted by plots in the GIS environment (Esri, 2022).

### Volume modeling

The variables derived from the images to apply modeling techniques were treated as independent variables and the volume per plot (m<sup>3</sup> 0.05 ha<sup>-1</sup>) as a dependent variable. Variables were submitted to Pearson’s correlation coefficient analysis to evaluate the degree of association between them. Vegetation indices and other adapted indices correlated with volume per plot (m<sup>3</sup> 0.05 ha<sup>-1</sup>) were used for modeling considering three scenarios: i) vegetation indices obtained from the Sentinel-2 image; (ii) adapted indices derived from

**Table 3.** Vegetation indices derived from a Sentinel-2 image for a *Pinus taeda* L. stand.

Vegetation index	Formula	Reference
Anthocyanin Reflectance Index - ARI1	$\frac{(1)}{(GREEN)} - \frac{(1)}{(REDE1)}$	Gitelson et al. (2001)
Anthocyanin Reflectance Index - ARI2	$\frac{(NIR)}{(GREEN)} - \frac{(NIR)}{(REDE1)}$	Gitelson et al. (2001)
Difference Vegetation-Index - DVI	NIR – RED	
Green Normalized Difference Index - GNDVI	$\frac{(NIR - GREEN)}{(NIR + GREEN)}$	Gitelson et al. (1996)
Inverted Red-Edge Chlorophyll Index - IRECI	$(REDE3 - RED) * \frac{(REDE2)}{(REDE1)}$	Clevers et al. (2000)
Modified Chlorophyll Absorption in Reflectance Index - MCARI	$\frac{(1 - 0,2 * (REDE1 - GREEN))}{(REDE1 - RED)}$	Daughtry (2000)
Modified Soil Adjusted Vegetation Index - MSAVI	$\frac{(NIR - RED)}{(NIR + RED + L)} (1 + L)$	Qi et al. (1994)
MERIS Terrestrial Chlorophyll Index - MTCI	$\frac{(REDE2 - REDE1)}{(REDE1 - RED)}$	Dash and Curran (2007)
Normalized Difference Index 45 - NDI45	$\frac{(REDE1 - RED)}{(REDE1 + RED)}$	Frampton et al. (2013)
Normalized Difference Vegetation Index - NDVI	$\frac{(NIR - RED)}{(NIR + RED)}$	Rouse et al. (1973)
Red-edge NDVI	$\frac{(NIR - REDE2)}{(NIR + REDE2)}$	Fernández-Manso et al. (2016)
Pigment Specific Simple Ratio – PSSRa	$\frac{(NIR)}{(RED)}$	Blackburn (1998)
Soil Adjusted Vegetation Index – SAVI	$1.5 * \frac{(NIR - RED)}{(NIR + RED + 0.5)}$	Huete (1988)
Sentinel-2 Red-Edge Position - S2REP	$740 * \frac{(0,5 * (REDE3 + RED) - REDE1)}{(REDE2 + REDE1)}$	Guyot and Baret (1988)

GREEN: 560 nm); RED: 665 nm; REDE1: red-edge 1 (705 nm); REDE2: red-edge 2 (740 nm); REDE3: red-edge 3 (783 nm); NIR: 842 nm; L: adjustment factor (considered as 0.5).

the Sentinel-1 image; iii) the combination of vegetation indices and adapted indices. The construction of regression models was based on the stepwise technique considering forward and backward modes in the R environment version 4.1.2. software program (R Core Team, 2021). To identify the best model, we applied the statistical criteria of highest adjusted coefficient of determination ( $R^2$  aj.), the low standard error value of the estimate ( $Syx\%$ ), and graphical analysis of the residuals, as recommended by Nicoletti *et al.* (2016), as well as low values of Akaike Information Criterion (AIC), Bayesian Information Criterion (BIC), and Root Mean Squared Error (RMSE).

**Statistical analysis**

First, the data derived from the Sentinel mission and estimated using forest inventory techniques were analyzed with the Shapiro-Wilk test to verify the basic assumptions of data normality. A completely randomized design was adopted with four treatments: T1) volume estimated by forest inventory techniques; T2) volume estimated by vegetation indices for Sentinel-2; T3) volume estimated by the indices adapted to Sentinel-1; and T4) volume estimated by the combination of Sentinel-1 and Sentinel-2 variables. Analysis of variance (ANOVA) was applied to identify the degree of significance of the treatments, and the Tukey’s test was used to assess whether there were significant differences between treatments. All statistical tests were performed in the R version 4.1.2. program (R Core Team, 2021).

**RESULTS**

The dendrometric characteristics of the evaluated stand based on the forest inventory performed in the area were: mean DBH: 26.3 cm; mean square diameter: 26.7 cm; mean total height: 17.4 meters; basal area per hectare: 39.8  $m^2.ha^{-1}$ ; total commercial volume per hectare: 228.5  $m^3.ha^{-1}$ , determined from the 5-degree tapering function (Schöpfer model) and cubic data of 72 trees from different diametric classes, as described in the methodology. Pearson’s correlation (Table 4) showed positive and negative correlations, with values ranging from -0.3621 to 0.3424. The vegetation indices and biophysical parameters from the Sentinel-2 image presented the highest values, while the indices adapted for the Sentinel-1 image had the lowest values.

The tested regression models presented different fitting metrics according to the variables used (Table 5). The models derived from the data extracted from the Sentinel-2 image were superior to the other models, with  $R^2$  adj. ranging from 0.51 to 0.40 and  $Syx\%$  between 3.66% to 8.97%. This was followed by the combination of the variables Sentinel-2 and Sentinel-1 ( $R^2$  adj. less than 0.30 and  $Syx\%$  above 10%). Finally, the models constructed with only Sentinel-1 variables presented the lowest fitting statistics.

The graphical analysis of the residuals (Figure 2) shows that there were no independent errors or under- or overestimates across all tested models. Models 1 and 2 presented the best metrics (highest  $R^2$  adj., and low  $Syx$  (%), AIC, and BIC), with uniform distribution of residuals and no outliers, unlike the other models.

**Table 4.** Pearson’s correlation coefficients between commercial volume and variables extracted from Sentinel-1 and Sentinel-2 images for a *Pinus taeda* L. stand.

Sentinel-1		Sentinel-2	
Variables	Pearson’s coefficient	Variables	Pearson’s coefficient
ARI1	-0.3622*	mRDFI	0.3317*
ARI2	-0.3275*	RVI	-0.2174*
CRI2	-0.3240*	RVIad	0.0130*
DVI	0.3425*	Ad_1	-0.0131*
FAPAR	0.3074*	Ad_2	-0.0132*
FVC	0.3355*	Ad_3	0.0008*
IAF	-0.3111*	Ad_4	0.0511*
IRECI	0.3174*	Ad_5	0.1031*
MCARI	0.2382*	-	-
MSAVI	0.2101*	-	-
NDI45	-0.0843*	-	-
NDVI	-0.1920*	-	-
NDVIR	-0.2063*	-	-
PSSRa	-0.0466*	-	-
SAVI	-0.2174*	-	-
SR	-0.2346*	-	-

Based on the statistical parameters described in Table 6 and the distribution of residuals (Figure 2), model 1 was chosen as the best regression model to estimate the commercial volume of the studied stand. Nevertheless, the statistical analyses show that the data have a normal distribution and that there are no significant differences between the volumes estimated by the treatments (volume estimated by the forest inventory; volume estimated by vegetation indices for Sentinel-2; volume estimated by the indices adapted for Sentinel-1; and volume estimated by the combined the variables Sentinel-1 and Sentinel-2; Table 6).

**DISCUSSION**

The correlation between the variables indicates that the indices formed by bands in the red-edge range for the Sentinel-2 image were more sensitive to the response variable analyzed. This is directly associated with the forest structure and the spectral bands used, as vegetation indices and texture variables may differ in their relationships with biomass and volume (Lu *et al.*, 2014). The correlation for the variables arising from the Sentinel-1 image was lower, which can be explained by the characteristics of the sensor, as the backscatter is dependent on surface characteristics, bandwidth (in this case, the C-band: 3.8 cm - 7.5 cm), and type of polarization (Maaya *et al.*, 2019). This can influence the degree of signal penetration in the forest, and consequently the degree of response obtained; the longer the wavelength, the greater the penetration capacity of the signals emitted from the vegetation canopy or the ground surface (Sano *et al.*, 2020).

**Table 5.** Regression models fitted to estimate the commercial volume of a *Pinus taeda* L. stand located in Rio Negro, Paraná, Brazil.

Model	Variables	Sensor	R <sup>2</sup> adj.	Syx (%)	AIC	BIC
1	ARI1, ARI2, CRI2 and FVC	Sentinel-2	0.51	3.6	134.8	185.3
2	ARI1, ARI2, CRI2 and IAF	Sentinel-2	0.48	3.7	138.0	186.7
3	ARI1, ARI2, CRI2 and SAVI	Sentinel-2	0.48	4.1	138.5	181.6
4	ARI1, ARI2, CRI2 and S2REP	Sentinel-2	0.47	3.7	138.6	181.6
5	ARI1, ARI2, CRI2 and GNDVI	Sentinel-2	0.47	6.9	139.3	184.2
6	ARI1, ARI2, CRI2 and MSAVI	Sentinel-2	0.46	8.9	139.6	188.2
7	ARI1, ARI2, CRI2 and FAPAR	Sentinel-2	0.45	5.5	140.8	191.4
8	S2REP, PSSRa, IRECI and NDI45	Sentinel-2	0.40	4.2	143.5	177.9
9	Ad_3, Ad_4, RVI and Ad_5	Sentinel-1	0.17	11.0	160.1	214.4
10	ARI2, FVC, mRDFI and Ad_1	Sentinel-1 and 2	0.29	10.5	150.3	178.4
11	ARI2, CRI2, mRDFI and Ad_2	Sentinel-1 and 2	0.26	10.1	155.2	198.3

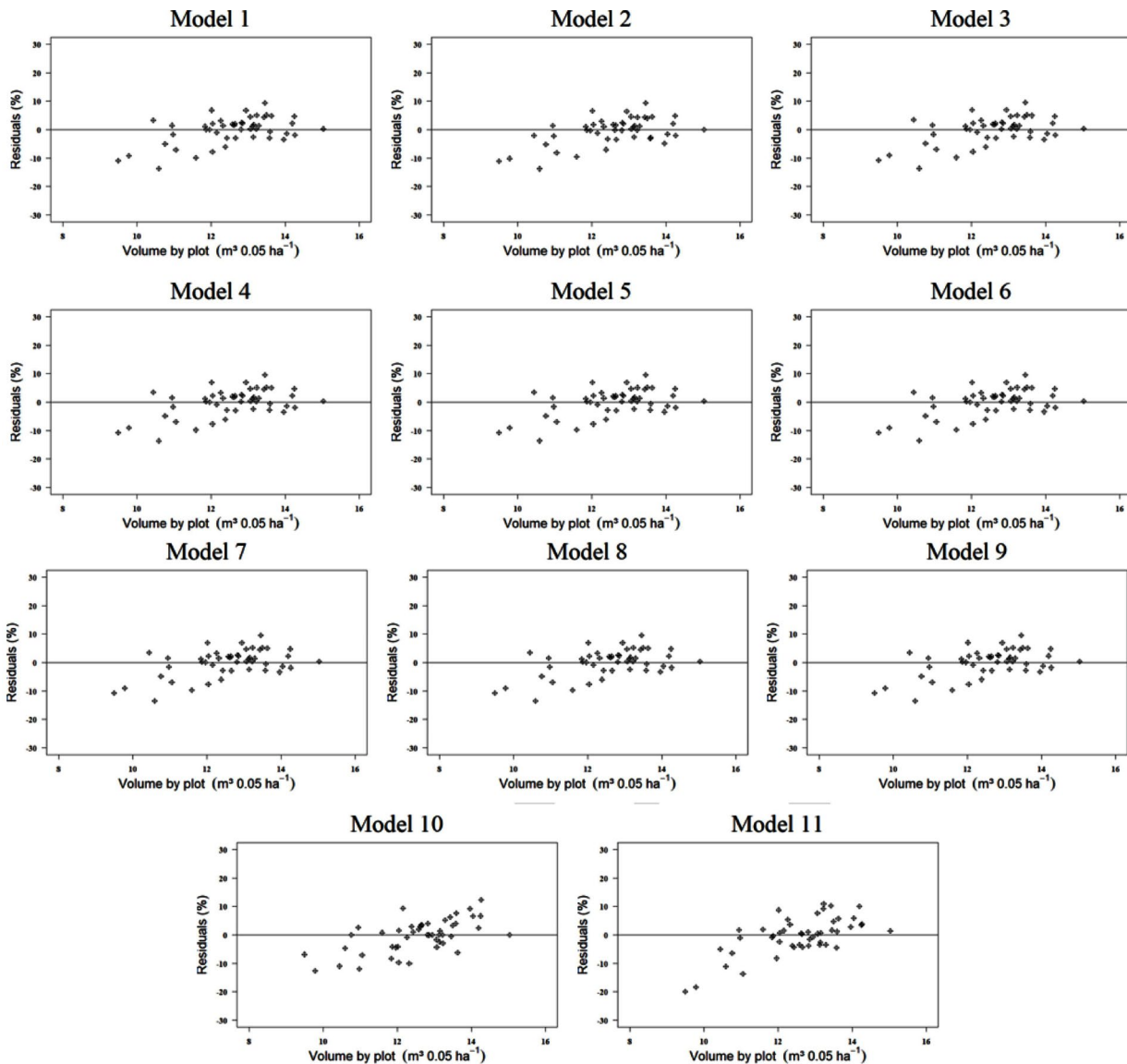


**Figure 2.** Distribution of residuals for models built with variables extracted from Sentinel-1 and Sentinel-2 images for a *Pinus taeda* L. stand.

**Table 6.** Estimated volume per plot (0.05 m<sup>3</sup>.ha<sup>-1</sup>) obtained through the forest inventory and remote data in *Pinus taeda* L. stand.

Treatments	v	V
T1 – Inventory	12.56	228,5
T2 – Sentinel-2	12.61	228,5
T3 – Sentinel-1	12.82	228,7
T4 – Sentinel-1 and Sentinel-2	12.71	228,7

v: average volume per plot (m<sup>3</sup>.0.05 ha<sup>-1</sup>); V: average volume per hectare (m<sup>3</sup>. ha<sup>-1</sup>).

Another important factor is the structure of the canopy of the stand. As Macedo et al. (2017) indicate, stands with closed canopies have positive correlations, while negative correlations are found in open canopies. In addition, the analyzed vegetation indices exploit the spectral bands, particularly in the visible and infrared range and in the red-edge range. According to Watzlawick et al. (2009), the near-infrared range (0.71 μm to 1.3 μm) presents the highest values of vegetation reflectance due to the cellular structures of the leaves. It is worth noting that the number of leaves and the architecture of the canopy directly influence the reflectance of forest stands (Ponzoni et al., 2012).

The graphical analysis of the residuals (Figure 1) shows that there were no independent errors and under- or overestimates across all tested models. Models 1 and 2 presented the best metrics (highest R<sup>2</sup> adj., and low Syx (%), AIC, and BIC), with uniform distribution of residuals and no outliers, unlike the other models. The forest stand volume is generally directly related to factors such as plant spacing, different ages, canopy architecture, and degree of canopy opening (Dai et al., 2021), despite the remote sensing data sources used. In relation to optical sensors (i.e. Sentinel-2), several studies aiming at volumetric estimates have been conducted mainly focusing on *Eucalyptus* spp. plantations. For example, Almeida et al. (2021) trained artificial neural networks with data on volume, age, bands, vegetation indices, and genetic material to estimate the volume of *Eucalyptus* plantations with a residual error of 10.63% to 12.00%.

The use of Sentinel-1 data in this study was not satisfactory, since the modeling resulting from these data did not present significant parameters. This is due to the limited sensitivity of the sensor to the different vegetation components, as the energy of the sensor that penetrated the vegetation and the amount of backscattering depend on the canopy structure (Eisfelder, et al. 2011). In addition to these variables, imaging geometry, range and azimuth resolution, relief distortion, Speckle noise, and the Doppler effect may also have contributed to this result (Meneses; Almeida, 2012).

Similar results were found in a study by Theofanous et al. (2021), in which Sentinel mission images were also used to estimate above-ground biomass for plantations in Greece using random forest models. The data were divided into monthly and seasonal time series; however, the inclusion of Sentinel-1 variables did not improve the estimates. The model with the greatest accuracy was only derived from Sentinel-2 spectral indices, with an R<sup>2</sup> of

0.52. The authors attribute this fact to the phenophases of the evaluated plantations and their relationship with the data sources considered in the study. Data from active sensors have been used in biomass mapping, especially in forest areas (Issa et al., 2020). However, the complexity of understanding and processing the information generated is still a challenge in such analyses. As such, the possibility of developing studies that integrate active and passive sensors is an important alternative for estimates of forest parameters, such as wood volume.

This is consistent with the study by Mauya et al. (2019), in which the capacities of Alos Palsar-2, Sentinel-1, and Sentinel-2 were assessed for volume prediction in small-scale forest plantations in Tanzania. Thus, models were constructed with the combination of Sentinel-1 and Sentinel-2 data through multiple linear regression (R<sup>2</sup> of 0.52 and RMSEr of 46.98%), and only Sentinel-2 data (R<sup>2</sup> of 0.63 and RMSEr of 42.03%) were superior to the models constructed using only Sentinel-1 data (R<sup>2</sup> of 0.18 and RMSEr of 59.48%). These results are similar to those found in the present study (R<sup>2</sup> of 0.1742), which corroborates the argument that the L-band has a longer wavelength that can penetrate deep into the forest, while the dominant scattering processes in the X- and C-bands (used in this study) occur at the surface of the canopy layer (Sano et al., 2020).

Due to the limitations of optical and SAR spatial sensors, Souza et al. (2019) tested data from Alos Avnir-2 and Alos Palsar to develop regression models using vector regression, artificial neural networks, and random forests to estimate forest volume for *Eucalyptus* spp. The most accurate model was based on the combination of variables of Alos Avnir-2 and Alos Palsar, with a R<sup>2</sup> of 0.926 and a mean square error of 11.007 m<sup>3</sup>.ha<sup>-1</sup>.

In addition to the limitations related to remote sensing data, the modeling technique used must also be considered. Only stepwise modeling was used in this study; however, models derived from machine learning have been employed in many studies with similar objectives. Given this context, we suggest the use of other modeling techniques in addition to stepwise to improve volumetric estimates using remote sensing variables and dendrometric characteristics of the stand. The study by Astola et al. (2021) shows that the combination of Sentinel-2 data with machine learning algorithms provided satisfactory estimates for volume in four forest districts in Finland. Data in the visible and infrared bands combined with the Canopy Height Model and topographic features as predictor variables generated estimates with a RMSE of 42.6%. The authors suggest that the inclusion of topographic and canopy variables with Sentinel-2 images is an effective methodology for disseminating the use of machine learning.

## CONCLUSION

Based on our results, we found no significant differences between the volumetric estimates derived from remote sensing data and forest inventory techniques. The best model was derived using only Sentinel-2 variables.

## AUTHORSHIP CONTRIBUTION

Project Idea: PCT

Database: PCT, DJM

Analysis: PCT, NMF, DJM

Writing: PCT, NMF, DJM

Review: PCT, NMF, DJM

## REFERENCES

ALASKA SATELLITE FACILITY – ASF. *ASF Data Search*. Available in: <https://search.asf.alaska.edu/#/>. Access: 28 feb. 2022.

ALMEIDA, A. A. A.; THIERSCH, M. F. B. M.; BERNARDI, L. K.; PÁDUA, F. A. de; ARTEAGA, A. J. M.; THIERSCH, C. R. Artificial neural networks and remote sensing for volumetric prediction in a Eucalyptus sp. plantation. *Research, Society and Development*, v. 10, n. 12, pág. e250101220466, 2021.

ALVARES, C. A.; STAPE, J. L.; SENTELHAS, P. C.; GONÇALVES, J. L. M.; SPAROVEK, G. Köppen's climate classification map for Brazil. *Meteorologische Zeitschrift*, v. 22, n. 6, pág. 711-728, 2013.

ASTOLA, H.; SEITSONEN, L.; HALME, E.; MOLINIER, M.; LÖNNQVIST, A. Deep Neural Networks with Transfer Learning for Forest Variable Estimation Using Sentinel-2 Imagery in Boreal Forest. *Remote Sensing*, v. 13, n.12, pág. 1-32, 2021.

BERRA, E. F.; BRANDELERO, C.; PEREIRA, R. S.; SEBEM, E.; GOERGEN, L. C. G.; BENEDETTI, ACP; LIPPERT, D. B. Estimativa do volume total de madeira em espécies de eucalipto a partir de imagens de satélite Landsat. *Ciência Florestal*, v. 22, n. 4, pág. 853-864, 2012.

BLACKBURN, G. A. Spectral indexes for estimating photosynthetic pigment concentrations: A test using senescent tree leaves. *International Journal of Remote Sensing*, v. 19, n. 4, pág. 657-675, 1998.

CLEVERS, J. G. P. W.; JONG, S. M. de; EPEMA, G. F.; ADDINK, E. A.; BOX, P. O. Meris and the Red-Edge Index. In 2nd EARSeL workshop, pág. 1-16, 2000.

ÇOLAK, E.; CHANDRA, M.; SUNAR, F. The use of multi-temporal sentinel satellites in the analysis of land cover/land use changes caused by the nuclear power plant construction. *International Archives of the Photogrammetry, Remote Sensing & Spatial Information Sciences*, 2019.

DAI, P. V. S.; BAIQ, F. H. R.; AZEVEDO, G.B; FAGUNDES, L. A.; TRENTO, A. C. S. Estimativa de volume de madeira baseada em índices de vegetação. *Scientia Forestalis*, v. 49, n. 129, pág. e3301, 2021.

DASH, J.; CURRAN, P. J. Evaluation of the MERIS terrestrial chlorophyll index (MTCI). *Advances in Space Research*, v. 39, n. 1, pág. 100-104, 2007.

DAUGHTRY, C. Estimating Corn Leaf Chlorophyll Concentration from Leaf and Canopy Reflectance. *Remote Sensing of Environment*, v. 74, n. 2, pág. 229-239, 2000.

EARTH EXPLORER. *USGS science for a changing world*. Available in: <https://earthexplorer.usgs.gov/>. Access: 28 feb. 2022.

EISFELDER, C.; KUENZER, C.; DECH, S. Derivation of biomass information for semi-arid areas using remote-sensing data. *Remote Sensing*, v. 33, n. 9, pág. 1-48, 2011.

EUROPEAN SPACE AGENCY-ESA. *ESA – Observing the Earth*. 2022a. Available in: [https://www.esa.int/Applications/Observing\\_the\\_Earth](https://www.esa.int/Applications/Observing_the_Earth). Access: 28 mar. 2022.

EUROPEAN SPACE AGENCY-ESA. *Sentinel-1 SAR technical guide*. 2022b. Available in: <https://sentinels.copernicus.eu/web/sentinel/technical-guides/sentinel-1-sar>. Access: 28 mar. 2022.

EUROPEAN SPACE AGENCY-ESA. *Sentinel-1 SNAP download*. 2022c. Available in: <https://step.esa.int/main/download/snap-download/>. Access: 28 mar. 2022.

FERNÁNDEZ-MANSO, A.; FERNÁNDEZ-MANSO, O.; QUINTANO, C. SENTINEL-2A red-edge spectral indexes suitability for discriminating burn severity. *International Journal of Applied Earth Observation and Geoinformation*, v. 50, pág. 170-175, 2016.

FERRO, F. S.; SILVA, D. A. L.; ICIMOTO, F. H.; LAHR, F. A. R.; GONZÁLIZ-GARCÍA, S. Environmental life cycle assessment of industrial pine roundwood production in Brazilian forests. *Science of the Total Environment*, v. 640-641, pág. 599-608, nov. 2018.

FLORES-ANDERSEN, A. I.; HERNDON, K. E.; THAPA, R. B.; CHERRINGTON, E. *The SAR Handbook: Comprehensive Methodologies for Forest Monitoring and Biomass Estimation*. 2019. 307 p.

FRAMPTON, W. F.; DASH, J.; MOUGH, G.; MILTON, E. J. Evaluating the capabilities of Sentinel-2 for quantitative estimation of biophysical variables in vegetation. *ISPRS Journal of Photogrammetry and Remote Sensing*, v. 82, pág. 83-92, 2013.

GITELSON, A. A.; KAUFMAN, Y. J.; MERZLYAK, M. N. Use of a green channel in remote sensing of global vegetation from EOS-MODIS. *Remote Sensing of Environment*, v. 58, n. 3, pág. 289-298, 1996.

GITELSON, A. A.; MERZLYAK, M.N; CHIVKUNOVA, O. B.; GITELSON, A. A; MERZLYAK, M. N; CHIVKUNOVA, O. B. Optical properties and nondestructive estimation of anthocyanin content in plant leaves. *Photochemistry and Photobiology*, v. 74, n. 1, pág. 38-45, 2001.

GUYOT, G.; BARET, F. Utilisation de la Haute Resolution Spectrale pour Suivre L'état des Couverts Vegetaux. In: 4th International Colloquium "Spectral Signatures of Objects in Remote Sensing", Aussois, Paris: ESA, n. 287, pág. 279-286, 1988.

HUETE, A. A soil-adjusted vegetation index (SAVI). *Remote Sensing of Environment*, v. 25, n. 3, pág. 295-309, 1988.

INDÚSTRIA BRASILEIRA DE ÁRVORES - IBÁ. *Relatório anual IBÁ – 2021*. Available in: <https://iba.org/datafiles/publicacoes/relatorios/relatorioiba2021-compactado.pdf> Access: 28 feb. 2022.

ISSA, S.; DAHY, B.; KSIKSI, T.; SALEOUS, N. A Review of Terrestrial Carbon Assessment Methods Using Geo-Spatial Technologies with Emphasis on Arid Lands. *Remote Sensing*, vol. 12, n.12, pág. 1-32, 2020.

LEAL, F. A.; MATRICARDI, E. A. T.; OLIVEIRA, K. A. de; ALMEIDA, G. S. Índice de vegetação na estimativa do volume em um povoamento de eucalipto. *Enciclopédia Biosfera*, v. 9, n. 17, pág. 1638-1646, 2013.

LU, D.; CHEN, Q.; WANG, G.; LIU, L.; LI, G.; MORAN, E. A survey of remote sensing based aboveground biomass estimation methods in forest ecosystems. *International Journal of Digital Earth*, v. 9, n. 1, pág. 63-105, 2016.

MACEDO, F. L.; SOUSA, A. M. O.; GONÇALVES, A. C.; SILVA, H. R.; RODRIGUES, R. A. F. Estimativa do volume de madeira para Eucalyptus sp. com imagens de satélite de alta resolução espacial. *Scientia Forestalis*, v. 45, n. 114, pág. 237-247, 2017.

MAUYA, E. W.; KOSKINEN, J.; TEGEL, K.; HÄMÄLÄINEN, J.; KAURANNE, T.; KÄYHKÖ, N. Modelling and Predicting the Growing Stock Volume in Small-Scale Plantation Forests of Tanzania Using Multi-Sensor Image Synergy. *Forests*, v.10, n.3, pág. 1-21, 2019.

MAUYA, EW; ENE, LT; BOLLANDSÅS, OM; GOBAKKEN, T; NÆSSET, E; MALIMBWI, RE; ZAHABU, E. Modelling aboveground forest biomass using airborne laser scanner data in the miombo woodlands of Tanzania. *Carbon Balance Management*, v. 10, n. 28, pág. 1-16, 2015.

MENESES, P. R.; ALMEIDA, T. D. *Introdução ao Processamento de Imagens de Sensoriamento Remoto*. Universidade de Brasília, Brasília, 2012, 266 p.

NICOLAU, A. P.; FLORES-ANDERSON, A.; GRIFFIN, R.; HERNDON, K.; MEYER, F. J. Assessing SAR C-band data to effectively distinguish modified land uses in a heavily disturbed Amazon Forest. *International Journal of Applied Earth Observation and Geoinformation*, v. 94, pág. 102214, 2021.

PONZONI, F. J.; SHIMABUKURO, Y. E.; KUPLICH, T. M. Sensoriamento remoto da vegetação. 2012. 135 p.

QI, J.; CHEBOUNI, A.; HUETE, A. R.; KERR, Y. H.; SOROOSHIAN, S. A modified soil adjusted vegetation index. *Remote Sensing of Environment*, v. 48, n. 2, pág. 119- 126, 1994.

ROUSE, J. W.; HAAS, R. H.; SCHELL, J. A. Monitoring the Vernal Advancement of Retrogradation (Green Wave Effect) of Natural Vegetation, Remote Sensing Center, Texas A&M University College Station, USA, 1974.

R CORE TEAM (2021). *R: A language and environment for statistical computing*. Vienna: R Foundation for Statistical Computing, Vienna, Austria. Available in: < <https://www.R-project.org/> >. Access: 28 fev. 2022.

SANO, E. E; MATRICARDI, E. A. T; CAMARGO, F. F. Estado da Arte do Sensoriamento Remoto de Radar: Fundamentos, Sensores, Processamento de Imagens e Aplicações. *Revista Brasileira de Cartografia*, v. 72, pág. 1458-1483, 2020.

SHAO, Z; ZHANG, L. Estimating forest aboveground biomass by combining optical and SAR data: A case study in Genhe, Inner Mongolia, China. *Sensors*, v. 16, n. 6, pág. 1-16, 2016.

SOUZA, GSA; et al Multi-sensor prediction of Eucalyptus stand volume: A support vector approach. *ISPRS Journal of Photogrammetry and Remote Sensing*, v. 156, pág. 135-146, 2019.

TORRES, R; et al Gmes sentinel-1 mission. *Remote Sensing of Environment*, v. 120, pág. 9-24, 2012.

TORRES, R; SNOEIJ, P; GEUPTNER, D; BIBBY, D; DAVIDSON, M; ATTENA, E; POTIN, P; ROMME, B; FLOURY, N; BROWN, M; TRAVER, I. N; DEGAYE, P; DUESMANN, B; ROSICH, B; MIRANDA, N; BRUNO, C; L'ABBATE, M; CROCI, R; PIETROPAOLO, A; HUCHLER, M, ROSTAN, F. *Remote Sensing of Environment*, v. 120, pág. 9-24, 2012.

THEOFANOUS, N; CHRYSAFIS, I; MALLINIS, G; DOMAKINIS, C; VERDE, N; SIAHALOU, S Aboveground Biomass Estimation in Short Rotation Forest Plantations in Northern Greece Using ESA's Sentinel Medium-High Resolution Multispectral and Radar Imaging Missions. *Forests*, v. 12, n. 7, pág. 902, 2021.

WATZLAWICK, L. F; KIRCHNER, F. F; SANQUETTA, C. R; Estimativa de biomassa e carbono em floresta com Araucaria utilizando imagens do satélite IKONOS II. *Ciência Florestal*, v. 19, n. 2, pág. 169-181, abr./jun. 2009.